

Comparison of the Internalization of Targeted Dendrimers and Dendrimer-Entrapped Gold Nanoparticles into Cancer Cells

Xiangyang Shi,^{1,2} Su He Wang,³ Inhan Lee,⁴ Mingwu Shen,² James R. Baker, Jr.³

¹ State Key Laboratory for Modification of Chemical Fibers and Polymer Materials, Donghua University, 2999 North Renmin Road, Shanghai 201620, People's Republic of China

² College of Chemistry, Chemical Engineering and Biotechnology, Donghua University, 2999 North Renmin Road, Shanghai 201620, People's Republic of China

³ Michigan Nanotechnology Institute for Medicine and Biological Sciences, University of Michigan, 109 Zina Pitcher Place, 4037 BSRB, Ann Arbor, MI 48109

⁴ Michigan Center for Biological Information and Department of Psychiatry, University of Michigan, 3600 Green Court, Suite 700, Ann Arbor, MI 48105

Received 8 May 2009; revised 14 June 2009; accepted 8 July 2009

Published online 14 July 2009 in Wiley InterScience (www.interscience.wiley.com). DOI 10.1002/bip.21279

ABSTRACT:

Dendrimer-based nanotechnology significantly advances the area of targeted cancer imaging and therapy. Herein, we compared the difference of surface acetylated fluorescein isocyanate (FI) and folic acid (FA) modified generation 5 (G5) poly(amidoamine) dendrimers (G5.NHAc-FI-FA), and dendrimer-entrapped gold nanoparticles with similar modifications ($[(Au^0)_{51.2}\text{-G5.NHAc-FI-FA}]$) in terms of their specific internalization to FA receptor (FAR)-overexpressing cancer cells. Confocal microscopic studies show that both G5.NHAc-FI-FA and $[(Au^0)_{51.2}\text{-G5.NHAc-FI-FA}]$ exhibit similar internalization kinetics regardless of the existence of Au nanoparticles (NPs). Molecular dynamics

simulation of the two different nanostructures reveals that the surface area and the FA moiety distribution from the center of the geometry are slightly different. This slight difference may not be recognized by the FARs on the cell membrane, consequently leading to similar internalization kinetics. This study underlines the fact that metal or inorganic NPs entrapped within dendrimers interact with cells in a similar way to that of dendrimers lacking host NPs. © 2009 Wiley Periodicals, Inc. *Biopolymers* 91: 936–942, 2009.

Keywords: dendrimers; gold nanoparticles; internalization; cancer cells

This article was originally published online as an accepted preprint. The "Published Online" date corresponds to the preprint version. You can request a copy of the preprint by emailing the *Biopolymers* editorial office at biopolymers@wiley.com

Correspondence to: Xiangyang Shi; e-mail: xshi@dhu.edu.cn, S. H. Wang; e-mail: shidasui@umich.edu, or J. R. Baker, Jr.; e-mail: jrbakerjr@umich.edu
X. Shi and S. H. Wang equally contributed to this work.

Contract grant sponsor: National Institutes of Health (NIH)

Contract grant numbers: NOI-CO-97111, 1 R01 CA119409, 1 R01 EB002657

Contract grant sponsor: The National Basic Research Program of China (973 Program)

Contract grant number: 2007CB936000

Contract grant sponsor: The Program for Professor of Special Appointment (Eastern Scholar) at Shanghai Institutions of Higher Learning and the National Cancer Institute (NCI)

© 2009 Wiley Periodicals, Inc.

INTRODUCTION

Dendrimers are a novel class of highly branched, monodispersed, synthetic macromolecules with defined composition and molecular architecture.^{1,2} The unique structural features of dendrimers allow for their many promising biomedical applications.

Recent advances in dendrimer-based nanomedicine show that dendrimers, especially poly(amidoamine) (PAMAM) dendrimers, can be covalently modified with targeting ligands, dyes, and drugs for targeted cancer imaging and therapeutics.^{3–6} To achieve multimodal imaging and therapy of cancer, dendrimers have been assembled onto magnetic iron oxide nanoparticles (NPs) for magnetic resonance imaging of tumors,^{7–9} or used to entrap gold (Au) NPs for subsequent cancer cell targeting and imaging.^{10–12} Both dendrimers and dendrimer/inorganic hybrid NPs can be biologically functionalized to be able to target cancer cells. This implies that through judicious manipulation, dendrimer/inorganic hybrid NPs could act in a way similar to dendrimers in terms of cancer cell targeting.

As a “soft” particle, a dendrimer molecule is quite flexible in aqueous solution; whereas, a dendrimer/inorganic hybrid NP could be considered a “hard” particle with very different hydrodynamic behavior than that of the dendrimer. It is reasonable to anticipate that the kinetics of cellular internalization could be very different even if both “soft” and “hard” particles bear similar targeting moieties or functional groups.

To fully understand the cellular targeting and uptake behavior of dendrimers and dendrimer/inorganic hybrid NPs, in this study we compared the difference between generation 5 (G5) PAMAM dendrimers and Au NPs entrapped within G5 dendrimers (or dendrimer-entrapped Au NPs, in short, Au DENPs) in terms of their targeting and internalization into cancer cells. Both G5 dendrimers and Au DENPs (Scheme 1) were modified to have similar surface targeting molecules [folic acid (FA)] and imaging molecules [fluorescein isocyanate (FI)]. KB cells (a human epithelial carcinoma cell line) which express a high level of FA receptors (FARs) were used as a model to carry out the experiment. The targeting and internalization of the G5 dendrimers and Au DENPs was monitored using laser confocal microscopy. The molecular structures of both G5 dendrimers and Au DENPs were modeled using molecular dynamics (MD) simulations in terms of the total surface area of the NPs and the FA distribution on the particle surfaces in order to delineate the related mechanism. The aim of this study is to compare the differ-

ence in the targeted cellular internalization between the “soft” dendrimer and “hard” DENP particles. Results of this study are expected to provide a fundamental understanding on how to rationally design dendrimer-based organic/inorganic hybrid nanodevices for biomedical applications. To our knowledge, this is the first study related to the comparison of dendrimers and dendrimer/metal hybrid NPs in terms of the kinetics of their targeting and uptake by cancer cells.

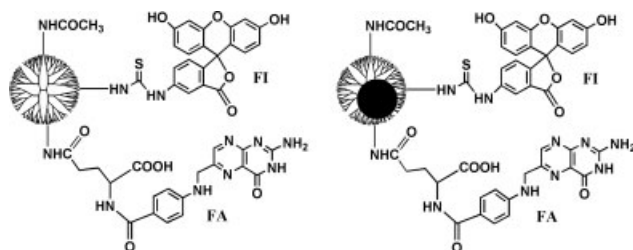
MATERIALS AND METHODS

Materials

Amine-terminated PAMAM dendrimers of generation 5 (G5.NH₂) with ethylenediamine core were purchased from Dendritech (Midland, MI) in methanol solution. The G5.NH₂ dendrimers were conjugated with FI and FA as described in our previous report.^{8,9} The remaining amines of the dendrimers were converted to acetyl groups by reacting with acetic anhydride according to previous reports.^{13–15} The synthesized FI- and FA-modified G5 dendrimers with acetylated surface groups are denoted as G5.NHAc-FI-FA. The average numbers of FI and FA moieties conjugated onto each dendrimer were estimated to be 4.5 and 4.8, respectively.^{8,9} Surface acetylated Au DENPs with both FI and FA modification ($[(Au^0)_{51.2}\text{-G5.NHAc-FI-FA}]$) were synthesized and characterized according to our another previous report.¹¹ The practical stoichiometry of gold/dendrimer was estimated to be 49.7 according to inductively coupled plasma atomic emission spectroscopy measurements, which is close to the theoretical value (51.2). Note that the synthesized $[(Au^0)_{51.2}\text{-G5.NHAc-FI-FA}]$ DENPs and the G5.NHAc-FI-FA dendrimers were from different batches. The average numbers of FI and FA moieties conjugated onto each Au DENP were estimated to be 4.0 and 4.5, respectively.¹¹ All other chemicals were obtained from Aldrich and used as received. The water used in all experiments was passed through a Millipore Milli-Q Plus 185 purification system and had a resistivity exceeding 18.2 M Ω cm.

Characterization of G5.NHAc-FI-FA Dendrimers

¹H-NMR spectrum of G5.NHAc-FI-FA dendrimers was recorded on a Bruker DRX 500 nuclear magnetic resonance spectrometer. Samples were dissolved in D₂O before NMR measurements. Matrix-assisted laser desorption ionization-time of flight (MALDI-TOF) mass spectrometry was performed using a Waters Tofspec-2E mass spectrometer (Beverly, MA) run in linear mode with the high mass PAD detector. Briefly, one milligram of a dendrimer sample was dissolved in 1 mL of methanol and then diluted with methanol to get the final dendrimer concentration of 0.2 mg/mL. Equal volumes of the dendrimer solution (0.2 mg/mL) and the matrix trihydroxyacetophenone (THAP) solution (10 mg/mL, dissolved in 50/50 water/acetonitrile) were well mixed. Then, a 1- μ L solution of this mixture was injected onto the target spots and evaporated to dryness. The instrument was calibrated with bovine serum albumin in THAP. The data was acquired and processed using MassLynx 3.5 software. The surface potential of functionalized dendrimers or Au DENPs was measured by a Malvern Zetasizer Nano ZS model ZEN3600 (Worcestershire, UK) equipped with a standard 633 nm laser.



SCHEME 1 Schematic representation of the dendrimers (left panel) and Au DENPs (right panel) modified with FI and FA.

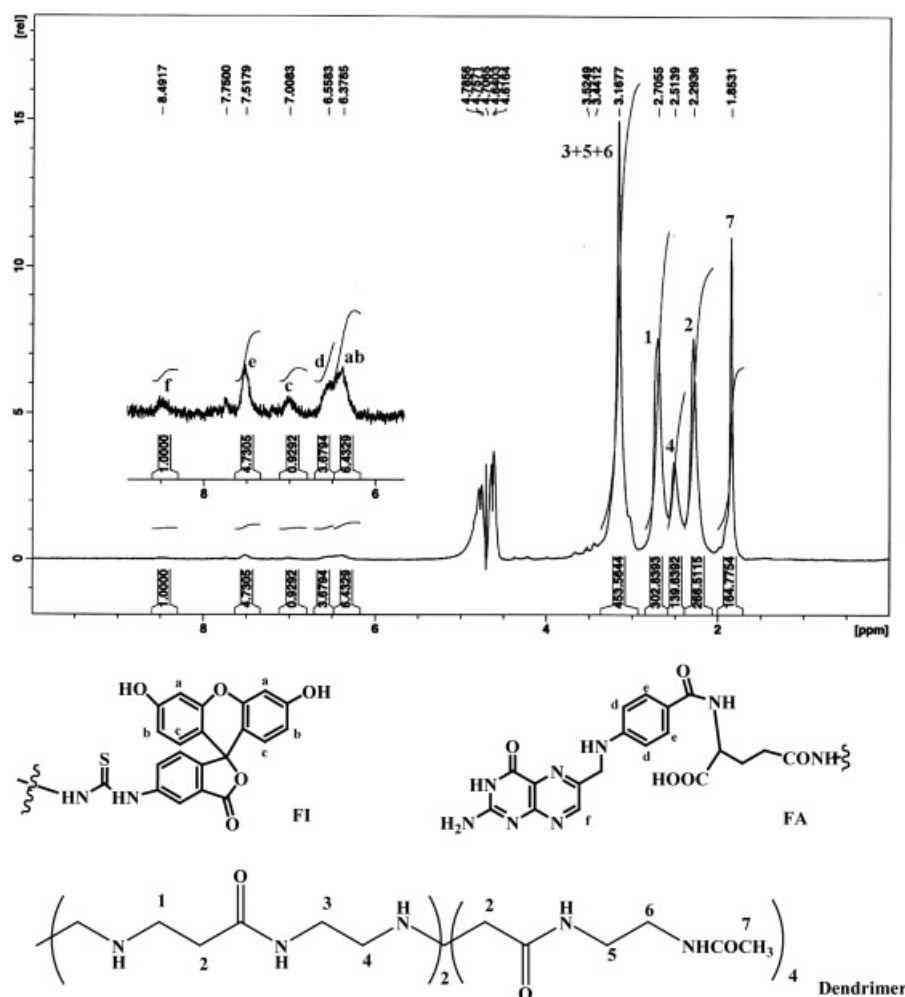


FIGURE 1 ¹H-NMR spectrum of the G5.NHAc-FI-FA dendrimers (top panel). Molecular structures of FI, FA, and dendrimers with NMR peak assignments are shown in the down panel.

Cell Cultures

The KB cells (ATCC, CLL17, Rockville, Maryland) were continuously grown in two 24-well plates, in FA-free RPMI 1640 medium (Gibco/BRL, Gaithersburg, Maryland) supplemented with penicillin (100 units/mL) (Sigma, St. Louis, Missouri), streptomycin (100 μ g/mL) (Sigma, St. Louis, Missouri), and 10% heat-inactivated FBS. The cells grown in FA-free media express a high level of FARs.

Confocal Microscopy

Confocal microscopic analysis was performed on cells (5×10^5 cells/dish) cultured on a glass bottom culture dish (MatTeK Corporation, Ashland, MA) using a Zeiss LSM 510-META laser scanning confocal microscope. FI fluorescence was excited with a 488-nm argon blue laser, and the emission was measured through a 505–525 barrier filter. The functionalized G5 dendrimers and Au DENPs were dissolved in PBS buffer to prepare concentrated stock solutions. The cells were incubated with functionalized G5 dendrimers (50 nM in RPMI 1640 medium) and Au DENPs (50 nM in RPMI 1640 medium), respectively for a time point of 1, 2, 6, and 24 h,

followed by rinsing with PBS buffer. The nuclei were counterstained with 1 μ g/mL of Hoescht33342, using a standard procedure. Samples were scanned using a 60 \times water immersion objective lens.

Molecular Dynamics Simulations

G5 dendrimers and Au DENPs with both FI and FA modifications were modeled and simulated under similar simulation conditions to those used in the previous studies (pH = 7).^{10,11} The conditions used best mimicked explicit water environment for PAMAM dendrimers according to our previous study.¹⁶ Five FI and five FA conjugation sites were randomly chosen among available terminal amines after G5.NH₂ was equilibrated. All models were built on an Onyx workstation (Silicon Graphics, Inc.; Mountain View, CA) using the Insight II software package (Accelrys, Inc.; San Diego, CA). Au spheres were configured as cubic close-packed structures, following their crystal structures. To mimic the synthesis steps, FA and FI attachment and acetylation were applied following entrapment of a metal sphere by an equilibrated G5.NH₂. Insight II software calculates total energy as bonded (U_{bonded} : empirical potential energy terms describing chemical bonds) and nonbonded

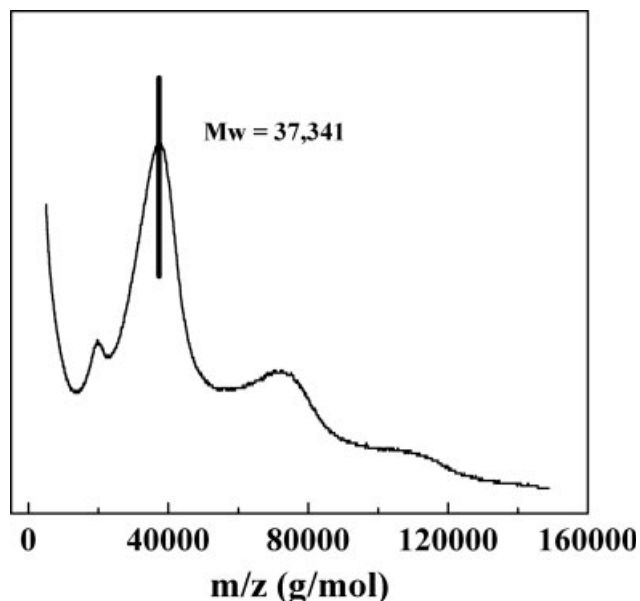


FIGURE 2 MALDI-TOF mass spectrum of the G5.NHAc-FI-FA dendrimers.

($U_{\text{nonbonded}}$: Lennard-Jones and Coulomb potential energy) interactions in MD simulations, such as

$$\begin{aligned}
 U_{\text{total}} &= U_{\text{bonded}} + U_{\text{nonbonded}} \\
 &= U_{\text{bonded}} + U_{\text{Lennard-Jones}} + U_{\text{Coulomb}} \\
 &= U_{\text{bonded}} + \frac{1}{2} \sum_i \sum_j \left\{ \varepsilon \left[\left(\frac{\sigma}{r} \right)^{12} - 2 \left(\frac{\sigma}{r} \right)^6 \right] + \frac{q_i q_j}{D r} \right\} \quad (1)
 \end{aligned}$$

where ε is the minimum energy of the Lennard-Jones potential; σ , the distance yielding minimum Lennard-Jones potential; q ,

the partial charge of the atom; D , the dielectric constant (1 for vacuum); r , the distance between i and j ; and i, j are non-bonded atom pairs. Based on previous findings, we used distance-dependent dielectric constant $D = r$ without a long-range interaction cut-off in the simulations.¹⁶ The dielectric constant D was not fixed. It was changing with the distance r . After 5000 steps of steepest descent minimization, MD simulations were performed at 1000 K for 5 ps followed by 100 ps runs with 1 fsec step at 300 K, using a consistent valence force field in Insight II software. The potential energies stabilized much earlier than 50 ps, and the mean values were calculated in simulation from 40 to 100 ps. The equilibration has been confirmed by monitoring not only the potential energy but also the time evolution of the radius of gyration and distance between the center of gold particle and the dendrimer center of mass. The radius of gyration, radial distribution, and surface areas of the molecules were calculated using Decipher module in the Insight II software.

RESULTS AND DISCUSSION

For targeted cancer cell imaging and uptake studies, it is crucial to prepare surface-neutralized NPs. Our previous studies show that an acetylation reaction can neutralize the positive amine-related surface charges of dendrimers⁵ or dendrimer/inorganic hybrid NPs,^{8–12,17} significantly improving the biocompatibility of the dendrimers or NPs and decreasing the nonspecific charge-based binding of cell membranes with the particles. In this study, the G5.NHAc-FI-FA dendrimers were synthesized by acetylation of amine-terminated G5.NH₂-FI-FA dendrimers, which were synthesized according to our previous reports.^{8,9} The average numbers of FI and FA

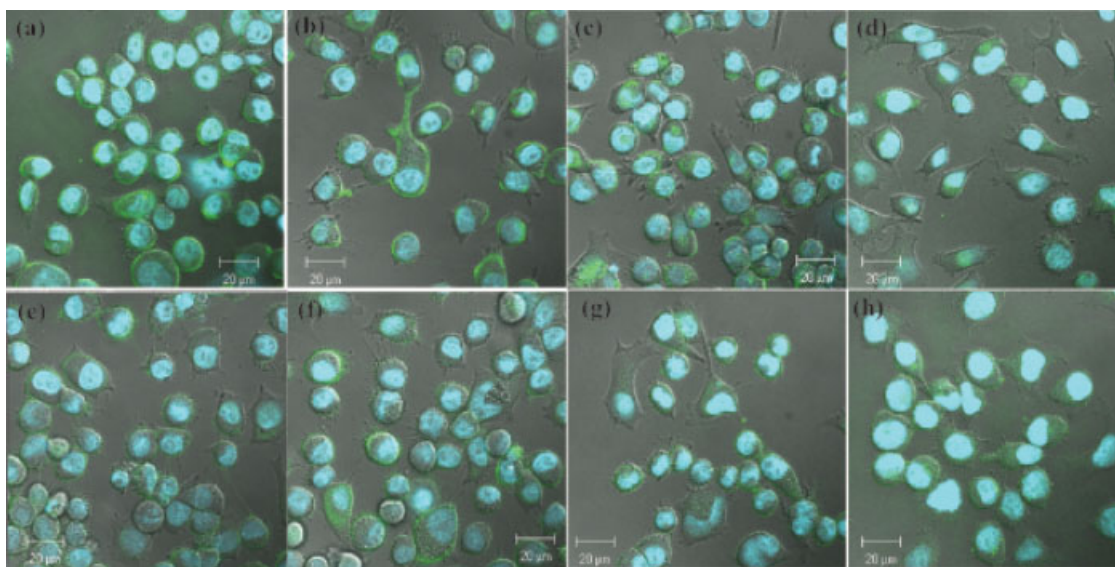


FIGURE 3 Laser confocal microscopy images of KB cells treated with the G5.NHAc-FI-FA dendrimers at 1 h (a), 2 h (b), 6 h (c), and 24 h (d) and KB cells treated with [(Au⁰)_{51.2}-G5.NHAc-FI-FA] DENPs at 1 h (e), 2 h (f), 6 h (g), and 24 h (h).

Table I Average Characteristic Values of the G5.NHAc-FI-FA Dendrimers and the [(Au⁰)_{51.2}-G5.NHAc-FI-FA] DENPs in Simulation Time from 40 to 100 ps

Materials	Metal Radius (nm)	R _g (nm)	Total Surface Area (nm ²)
G5.NHAc-FI-FA	0	2.03	126
[(Au ⁰) _{51.2} -G5.NHAc-FI-FA]	1.5	2.21	153

conjugated onto each G5 dendrimer were determined to be 4.5 and 4.8, respectively.^{8,9} ¹H-NMR was used to confirm the structural conversion of the dendrimer terminal amine groups to acetyl groups (Figure 1). The prominent NMR peak at 1.85 ppm is related to the proton signal of the —COCH₃ terminal groups. However, the aromatic proton peaks related to both FI and FA did not show any significant changes compared with the ¹H-NMR spectrum of the G5.NH₂-FI-FA dendrimers.⁹ Zeta-potential measurements show that after the acetylation reaction, the surface potentials of the G5.NH₂-FI-FA (+30.3 mV) dendrimers significantly decreased when G5.NHAc-FI-FA (−1.66 mV) dendrimers were formed, further confirming the successful transformation of the dendrimer terminal amines to acetamide groups. The slightly negative charges may derive from the deprotonated carboxyl groups in both FI and FA moieties being conjugated. The zeta-potential value of G5.NHAc-FI-FA dendrimers is approximately similar to that of [(Au⁰)_{51.2}-G5.NHAc-FI-FA] DENPs (−2.30 mV),¹¹ indicating that the presence of Au NPs inside the dendrimers does not significantly affect the surface charge of the particles.

The molecular weight of G5.NHAc-FI-FA dendrimers was measured to be 37,341 using MALDI-TOF mass spectrometry (Figure 2). Due to the entrapment of Au NPs, we have technical difficulty to obtain the MALDI spectrum of the

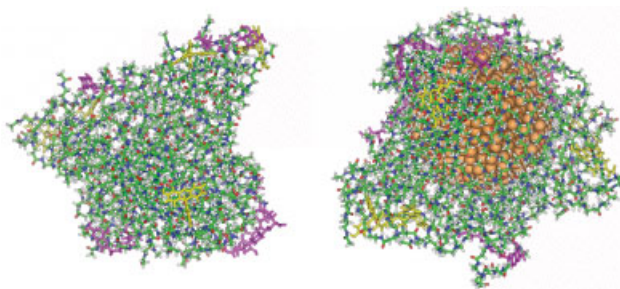


FIGURE 4 Equilibrated configurations of G5.NHAc-FI-FA dendrimers (left) and [(Au⁰)_{51.2}-G5.NHAc-FI-FA] DENPs (right) after 100 ps molecular dynamics simulations. The yellow and pink moieties on both configurations represent FI and FA molecules, respectively.

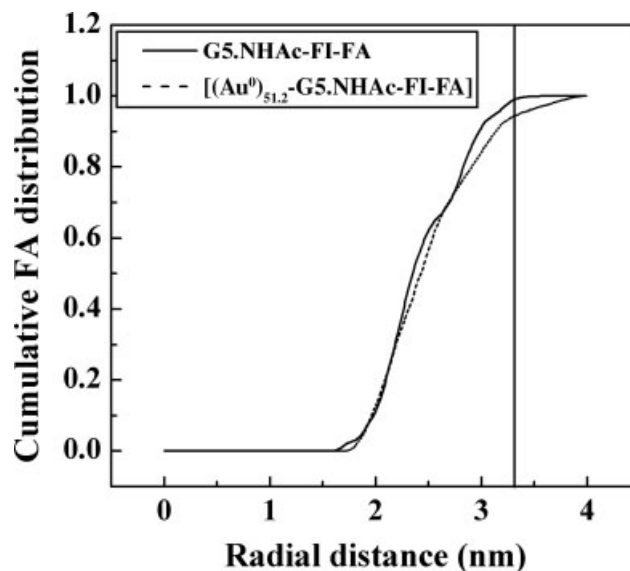


FIGURE 5 The cumulative normalized number distribution of FA moieties of the G5.NHAc-FI-FA dendrimers and the [(Au⁰)_{51.2}-G5.NHAc-FI-FA] DENPs as a function of the radial distance from the CM of the particle between 40 and 100 ps simulation time. Vertical line shows the 3.3 nm radial distance.

corresponding Au DENPs. Therefore, the Mw of the Au DENPs was estimated to be the sum of the Mw of G5 dendrimers and the atomic weight of 51.2 Au atoms. The peaks on the left and the right of the main peak (37,341) should be related to the trailing generation and the dimers of the G5 dendrimers, which are often observed in MALDI spectra of PAMAM dendrimers.^{18,19} Although the polydispersity of dendrimers is very narrow when compared with traditional synthetic polymers, the molar mass fractions of dendrimers with generation larger than three in MALDI-TOF spectra are always broad. This has been demonstrated in literature.^{15,20} According to literature method,^{15,18–20} the average Mw data of dendrimers are often estimated at the center of the major mass fraction peaks. Therefore, we estimated the Mw of our functionalized G5 dendrimers to be 37,341. The numbers of FI and FA moieties attached onto each G5.NHAc-FI-FA dendrimer are approximately similar to those attached onto each [(Au⁰)_{51.2}-G5.NHAc-FI-FA] DENP.^{8,9,11} This ensures the reasonable comparison of their targeting and internalization to cancer cells. It has been demonstrated earlier that a dendrimer nanodevice with higher average number of folate (e.g., 7.2, 11.5, and 13.7) shows similar cellular uptake to that having average 4.7 folates.²¹ Therefore, in this study, we chose to use the dendrimer and the Au DENP nanodevice with average 4.8 and 4.5 folates on the surface, respectively for the comparison.

The targeting and uptake of G5.NHAc-FI-FA dendrimers and [(Au⁰)_{51.2}-G5.NHAc-FI-FA] DENPs to KB cells overexpressing FARs was monitored using confocal microscopic imaging through the linked FI dye molecules (Figure 3). We show that at the 1-h time point, both dendrimers and DENPs are dominantly located at the cell membrane surface (Figures 3a and 3e). A significant portion of both particles are internalized into KB cells at the 2-h time point (Figures 3b and 3f). At the 6-h and 24-h time points, both dendrimers and DENPs are almost completely internalized into the cells (Figures 3c, 3d, 3g, and 3h). We do not see any significant difference between dendrimers and DENPs in terms of the internalization kinetics, implying that the entrapped Au NPs (diameter = 3.2 nm)¹¹ inside the dendrimers for DENPs do not have an appreciable effect on the cellular uptake of the particles. It is noted that the location of the green fluorescence signal (inside the cells or onto the cell membrane surfaces) originating from FITC, which was conjugated onto both dendrimers and DENPs was used to judge whether or not the dendrimers or DENPs were internalized. Our imaging data show that there is no significant difference between (a) and (e), (b) and (f), (c) and (g), and (d) and (h), indicating that the internalization kinetics of targeted dendrimers and DENPs are more or less similar. We realize that it is important to quantify the confocal imaging data. However, to our best knowledge, currently there is no such a method allowing us to quantify the imaging data.

To further delineate the internalization of G5.NHAc-FI-FA dendrimers and [(Au⁰)_{51.2}-G5.NHAc-FI-FA] DENPs to KB cells, MD simulations were performed to compare the structural difference of the dendrimers and the DENPs. Table I lists the average characteristic values of the simulations. The radius of gyration (R_g) of G5.NHAc-FI-FA dendrimers and [(Au⁰)_{51.2}-G5.NHAc-FI-FA] DENPs were 2.0 and 2.2 nm, respectively. The total surface areas of the dendrimers and DENPs were 126 and 153 nm², respectively. A representative configuration of the dendrimers and the DENPs is shown in Figure 4. It is clear that an Au NP is completely entrapped within a single dendrimer molecule with FI and FA modified on the surface. The entrapment of Au NPs slightly increases the total surface area and the radius of gyration of the entire particle when compared with the FI- and FA-modified G5.NHAc-FI-FA dendrimers without Au NPs.

For cancer cell targeting and uptake, it is necessary to compare the difference of the FA distribution on both the dendrimers and the DENPs. The cumulative normalized number distribution of FA moieties during simulation time from 40 and 100 ps are shown in Figure 5 as a function of the radial distance from the center of mass (CM) of the particle. Both G5.NHAc-FI-FA dendrimers and [(Au⁰)_{51.2}-

G5.NHAc-FI-FA] DENPs have approximately similar FA position distribution from the center of the geometry. Only less than 4.6% of FA moieties of the [(Au⁰)_{51.2}-G5.NHAc-FI-FA] DENPs reaches farther out than FA moieties of the G5.NHAc-FI-FA dendrimers as shown with vertical line at 3.3 nm in Figure 5, where FA starts to be absent in G5.NHAc-FI-FA dendrimers. This suggests that the entrapment of Au NPs does not seem to significantly affect the FA distribution on the particle surfaces. It is interesting to note that since the hydrodynamic radius of G5 dendrimers is 2.7 nm,^{2,22} and the FA modification on dendrimers does not significantly increase the dendrimer hydrodynamic radius, we think that the range of the radial distance from the CM of the particle at 0–3.99 nm is sufficient for illustrating the FA position distribution. In practice, the slight increase of the total surface area for the [(Au⁰)_{51.2}-G5.NHAc-FI-FA] DENPs when compared with the G5.NHAc-FI-FA dendrimers may not be recognized or differentiated by FARs on the cell surface. Consequently, both G5.NHAc-FI-FA dendrimers and the [(Au⁰)_{51.2}-G5.NHAc-FI-FA] DENPs act similarly in terms of targeting and internalization to cancer cells through receptor-mediated endocytosis, which was confirmed by confocal microscopic imaging studies.

In summary, we have compared the targeting and internalization of the G5.NHAc-FI-FA dendrimers and the [(Au⁰)_{51.2}-G5.NHAc-FI-FA] DENPs to cancer cells expressing a high level of FARs. Our results show that regardless of the entrapment of Au NPs, both particles display similar kinetics of targeting and internalization. MD simulations reveal that the entrapment of Au NPs for DENPs slightly increases the total surface area and radius of gyration of the particles when compared with the dendrimers with similar surface modifications. However, the distribution of FA positions from the center of the geometry does not change significantly. Consequently, both particles with or without the entrapment of Au NPs display similar internalization kinetics to cancer cells through receptor-mediated endocytosis. Findings from this study are beneficial for the rational design and synthesis of various multifunctional dendrimer/metal hybrid nanodevices for a range of biomedical applications.

The authors thank Dr. Xiangdong Bi for his help with NMR experiments.

REFERENCES

1. Newkome, G. R.; Moorefield, C. N.; Vogtle, F. *Dendritic Molecules: Concepts, Syntheses, Perspectives*; Wiley-VCH: New York, 1997.
2. Tomalia, D. A.; Frechet, J. M. J. *Dendrimers and Other Dendritic Polymers*; John Wiley & Sons Ltd: New York, 2001.

3. Kukowska-Latallo, J. F.; Candido, K. A.; Cao, Z. Y.; Nigavekar, S. S.; Majoros, I. J.; Thomas, T. P.; Balogh, L. P.; Khan, M. K.; Baker, J. R., Jr. *Cancer Res* 2005, 65, 5317–5324.
4. Majoros, I. J.; Myc, A.; Thomas, T.; Mehta, C. B.; Baker, J. R., Jr. *Biomacromolecules* 2006, 7, 572–579.
5. Majoros, I. J.; Thomas, T. P.; Mehta, C. B.; Baker, J. R., Jr. *J Med Chem* 2005, 48, 5892–5899.
6. Thomas, T. P.; Majoros, I. J.; Kotlyar, A.; Kukowska-Latallo, J. F.; Bielinska, A.; Myc, A.; Baker, J. R., Jr. *J Med Chem* 2005, 48, 3729–3735.
7. Shi, X.; Thomas, T. P.; Myc, L. A.; Kotlyar, A.; Baker, J. R., Jr. *Phys Chem Chem Phys* 2007, 9, 5712–5720.
8. Shi, X.; Wang, S. H.; Swanson, S. D.; Ge, S.; Cao, Z.; Van Antwerp, M. E.; Landmark, K. J.; Baker, J. R., Jr. *Adv Mater* 2008, 20, 1671–1678.
9. Wang, S.; Shi, X.; Van Antwerp, M.; Cao, Z.; Swanson, S. D.; Bi, X.; Baker, J. R., Jr. *Adv Funct Mater* 2007, 17, 3403–3050.
10. Shi, X.; Lee, I.; Baker, J. R., Jr. *J Mater Chem* 2008, 18, 586–593.
11. Shi, X.; Wang, S.; Meshinchi, S.; Van Antwerp, M.; Bi, X.; Lee, I.; Baker, J. R., Jr. *Small* 2007, 3, 1245–1252.
12. Shi, X.; Wang, S.; Sun, H.; Baker, J. R., Jr. *Soft Matter* 2007, 3, 71–74.
13. Majoros, I. J.; Keszler, B.; Woehler, S.; Bull, T.; Baker, J. R., Jr. *Macromolecules* 2003, 36, 5526–5529.
14. Shi, X.; Banyai, I.; Rodriguez, K.; Islam, M. T.; Lesniak, W.; Balogh, P.; Balogh, L. P.; Baker, J. R., Jr. *Electrophoresis* 2006, 27, 1758–1767.
15. Shi, X.; Lesniak, W.; Islam, M. T.; Muñiz, M. C.; Balogh, L.; Baker, J. R., Jr. *Colloids Surf A* 2006, 272, 139–150.
16. Lee, I.; Athey, B. D.; Wetzel, A. W.; Meixner, W.; Baker, J. R., Jr. *Macromolecules* 2002, 35, 4510–4520.
17. Shi, X.; Sun, K.; Baker, J. R., Jr. *J Phys Chem C* 2008, 112, 8251–8258.
18. Bi, X.; Shi, X.; Baker, J. R., Jr. *J Biomater Sci Polym Ed* 2008, 19, 131–142.
19. Bi, X.; Shi, X.; Shukla, R.; Majoros, I. J.; Baker, J. R., Jr. *J Comput Theor Nanosci* 2007, 4, 1179–1187.
20. Woller, E. K.; Cloninger, M. J. *Biomacromolecules* 2001, 2, 1052–1054.
21. Hong, S.; Leroueil, P. R.; Majoros, I. J.; Orr, B. G.; Baker, J. R., Jr.; Banaszak Holl, M. M. *Chem Biol* 2007, 14, 107–115.
22. Tomalia, D. A.; Naylor, A. M.; Goddard, W. A., III. *Angew Chem Int Ed* 1990, 29, 138.

Reviewing Editor: Eric Toone